RESEARCH ARTICLE

National Science Open
5: 20250076, 2026
https://doi.org/10.1360/nso/20250076

Physics

THz single-shot optical imaging with tunable time interval

Qiyun Yao[1,#], Kaining Yang[1,#], Zhuo Yin[1], Xiaoya Ma[1], Quanxing Zhai[1], Mingjie Yu[1], Wenbin Yi[1], Hongwei Chen[2], Du Wang[1,*] & Cheng Lei[1,3,*]

[1]*School of Integrated Circuits, Wuhan University, Wuhan 430072, China;*
[2]*Department of Electronic Engineering, Tsinghua University, Beijing 100084, China;*
[3]*Shenzhen Institute of Wuhan University, Shenzhen 518057, China*

#Contributed equally to this work.
*Corresponding authors (emails: wangdu@whu.edu.cn (Du Wang); leicheng@whu.edu.cn (Cheng Lei))

Received 11 November 2025; Revised 10 February 2026; Accepted 13 May 2026; Published online 18 June 2026

Abstract: Single-shot multi-frame ultrafast optical imaging is a powerful tool for probing transient phenomena. However, in many ultrafast processes, the rate of temporal evolution varies with time, making conventional equal-interval imaging face a trade-off between temporal resolution and observation window. Here, by utilizing the wavelength-time duality of ultrashort pulses established by optical time-stretch, we generate a pulse sequence with arbitrarily tunable time intervals through spectral modulation. This enables adaptive sampling, i.e., dense sampling for high-dynamic stages and sparse sampling for slow evolution. The observation of laser filament dynamics in air shows that the system achieves 10-frame single-shot imaging with adjustable frame intervals from 0.26 to 2.12 ps. We expect that the proposed method can be readily incorporated into a wide spectrum of single-shot multi-frame ultrafast imaging systems, thereby advancing our capability to probe ultrafast phenomena.

Keywords: ultrafast imaging, ultrafast photonics, tunable time-interval, transient processes, single-shot

INTRODUCTION

Investigating ultrafast phenomena on timescales ranging from femtoseconds to nanoseconds is crucial for understanding and manipulating the material world, particularly for irreversible or difficult-to-replicate physical, chemical, and biological processes [1–6], such as material damage [7], irreversible chemical reactions [8], laser-induced shock waves [9], and laser-driven inertial confinement fusion [10,11]. Among various observation techniques, optical imaging, particularly single-shot multi-frame ultrafast optical imaging, has become one of the most important tools due to its unique combination of single-shot capture capability, high temporal resolution, and contactless observation.

Nowadays, there have been a number of representative techniques utilizing ultrashort laser pulses to achieve single-shot multi-image imaging, such as compressed ultrafast photography (CUP) [12–14], frequency recognition algorithm for multiple exposures (FRAME) [15,16], and Sequentially Timed All-optical Mapping Photography (STAMP) [17,18]. CUP achieves single-shot imaging with a frame rate of approximately 100 trillion frames per second and a sequence depth of hundreds of frames through compressed

© The Author(s) 2026. Published by Science Press and EDP Sciences. This is an Open Access article distributed under the terms of the Creative Commons Attribution License (https://creativecommons.org/licenses/by/4.0), which permits unrestricted use, distribution, and reproduction in any medium, provided the original work is properly cited.

acquisition followed by computational reconstruction [11]. FRAME achieves single-shot imaging with a temporal resolution of 200 fs through frequency-domain encoding combined with compressed sensing, enabling the reconstruction of ultrafast dynamic events [16]. STAMP achieves single-shot multi-frame imaging with a capability of 25 frames and a frame rate of 2.5 Tfps through spatio-temporal encoding, and enables real-time phase dynamics capture [14,19,20]. Although these methods each have their own advantages, the temporal evolution rates in real physical processes are not constant. This inherent variability creates an irreconcilable conflict between temporal resolution and observation window for ultrafast imaging techniques employing fixed time-interval sampling, thereby limiting their applications.

To address this limitation, we developed a single-shot ultrafast imaging system with tunable frame intervals named Tunable Time-interval STAMP (TT-STAMP) by combining the fundamental principles of the STAMP system. This system utilizes spatial dispersive elements and spatial light modulators to precisely control pulse parameters, achieving spectral modulation of femtosecond pulses and generating programmable sub-pulse sequences with specific time intervals [21]. Subsequently, by further applying the wavelength-frame division principle, we realized flexible temporal control in single-shot ultrafast imaging. Finally, we validated the system by reconstructing the ultrafast dynamics of laser-induced plasma filaments, demonstrating single-shot 10-frame ultrafast optical imaging with a 150 μm × 1 mm field of view and adjustable frame intervals ranging from 0.26 to 2.12 ps. We believe our method can be applied to various frequency-encoded single-shot multi-frame ultrafast imaging systems, thereby enhancing our observation capabilities for ultrafast processes.

MATERIALS AND METHODS

Principle

The overall architecture of TT-STAMP is illustrated in Figure 1. To achieve variable inter-frame interval imaging, we employed a femtosecond pulsed laser source characterized by a broad spectral range and extremely narrow pulse width, which was separated into multiple sub-pulses. These sub-pulses underwent manipulation to generate an ultrashort pulse sequence with flexible control over both pulse quantity and temporal intervals.

First, a dispersive element spatially dispersed the polychromatic pulse light, establishing a mapping relationship between spectral components and spatial positions. Subsequently, a phase modulation device applied distinct phase modulations to different spectral components, introducing specific time delays between them. After modulation, the monochromatic beams were recombined via a grating. Due to the new phase profile, the recombined light coherently reconstructed, causing the single pulse to temporally split into sub-pulses corresponding to different wavelength ranges, thus forming the modulated pulse sequence.

This sequence is then incident on the target to encode ultrafast information; crucially, as wavelengths are temporally arranged according to predefined sequences, each wavelength encodes ultrafast dynamics at distinct time points. Finally, a spatial mapping device (SMD) projects different wavelengths onto distinct detector positions, enabling acquisition of ultrafast phenomena imaging results across sequential time frames.

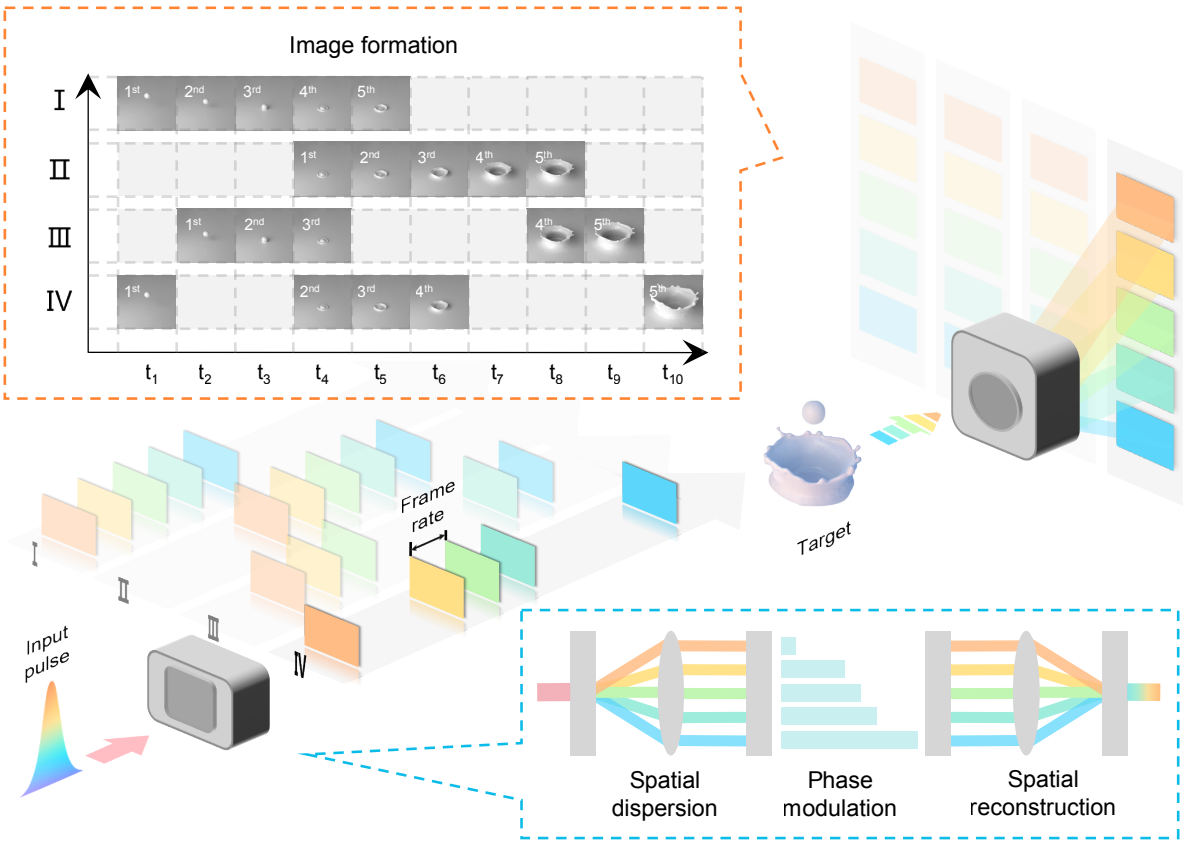

Figure 1 The architecture of TT-STAMP. The ultrashort laser pulse is first spatially dispersed, with each spectral component loaded with different phase modulations, before being recombined. The recombined spectral components will generate specific time intervals between them, forming a pulse sequence with non-uniform time intervals. By using this pulse sequence to encode ultrafast phenomenon information and then projecting it onto different spatial positions of the sensor through a spatial mapping device (SMD), we can obtain an ultrafast information sequence with variable time intervals.

Methods

Following the approach, we employed a femtosecond pulsed laser with a central wavelength of 800 nm, spectral bandwidth of 40 nm, and pulse width of 35 fs for the experiments. The specific experimental light path diagram is shown in Figure 2.

The pulse emitted from the laser was first split by a non-polarizing beam splitter (BS1) into pump light and probe light. The red line represents pump light and the blue line represents probe light.

The pump light passed through Time delay 1 and was focused onto the sample surface using lens 1 (f = 50 mm) to generate ultrafast phenomena. The probe light was temporally stretched using a glass rod (H-ZF12, 350 mm, GVD = 0.18 ps/nm) to serve as the overall observation time window. Theoretically, for our light source with a 40-nm spectral bandwidth, the pulse width broadens to 7.2 ps. Subsequently, it underwent spatial dispersion via diffraction grating 1 (1200 lines/mm, 25 mm × 25 mm), and cylindrical lens 1 (f = 150 mm) projected the spatially dispersed beam as spectral lines onto specific regions of a liquid crystal spatial light modulator (LC-SLM, HDSLM80R Plus, UPOLabs). The LC-SLM controls the orientation of liquid crystal molecules via electrical signals, utilizing their birefringence to alter the refractive index of

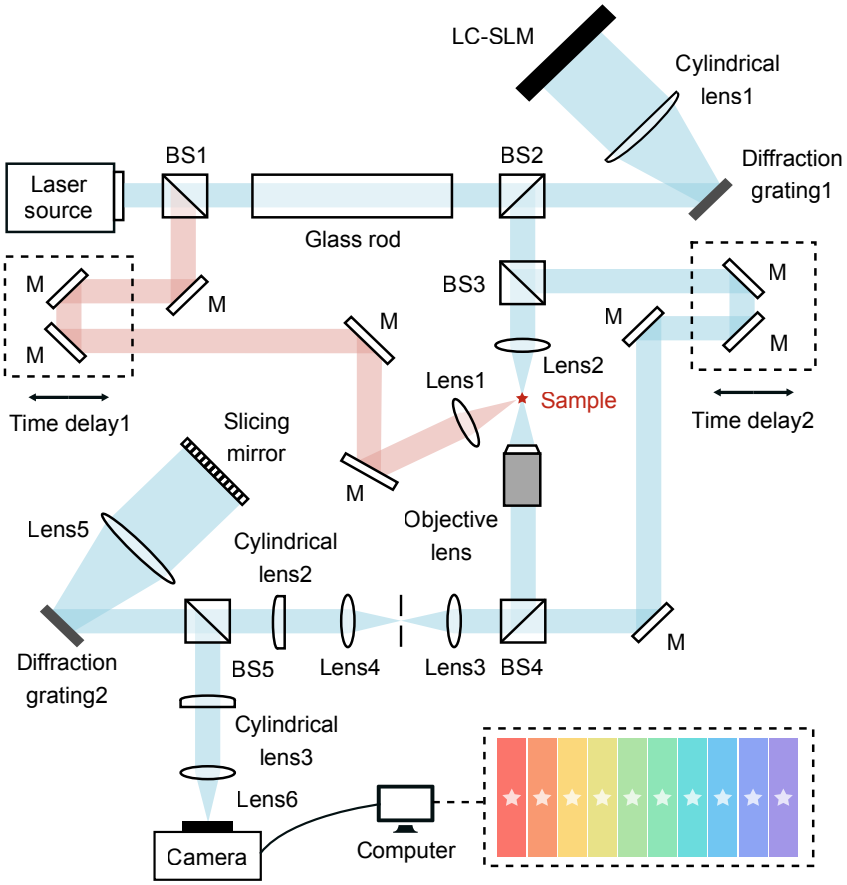

Figure 2 The specific experimental light path diagram. BS: beam splitter. M: mirror.

incident light. This enables precise phase delay modulation of the optical wavefront at each pixel. In experiments, by loading a phase modulation pattern onto the LC-SLM, distinct phase shifts are applied to different spatial regions. Subsequent beam recombination generates a pulse sequence with precisely controlled temporal intervals. Through this approach, loading different phase modulation patterns onto the LC-SLM produces pulse sequences with varying inter-pulse delays, corresponding to the four distinct frame-interval effects (Groups I–IV) illustrated in Figure 1.

The modulated probe light illuminated the sample region where ultrafast phenomena occurred and carried the ultrafast information; it was subsequently collected by an objective lens (NA = 0.28, 10×), and then recombined with the reference light at BS4. The combined beam was adjusted for field-of-view using lens 3 (f = 200 mm), an aperture, and lens 4. The light carrying ultrafast information was dispersed by diffraction grating 2, shaped by lens 5 (f = 150 mm), and projected onto a slicing mirror for spatial framing. Finally, pulses reflected from the slicing mirror were projected onto distinct regions of a camera [4], where each region represented ultrafast phenomena at different time points, enabling acquisition at specified temporal intervals.

Thus, unlike existing ultrafast imaging techniques based on equally-spaced pulse sequences, the core innovation of our work lies in the flexible and precise control of variable-interval pulse sequences. This was

achieved by individually applying specific phase modulations to pre-separated sub-pulses via the spatial light modulator.

RESULTS

To demonstrate the capability of the LC-SLM in controlling temporal pulse intervals, we measured autocorrelation signals of laser pulses under different modulation intervals, as shown in Figure 3.

Temporal resolution test of TT-STAMP

Figure 3(a) and (b) displays the autocorrelation signals of the original pulse emitted from the laser and the pulse after glass-rod stretching, respectively. The calculated pulse width of the original laser pulse was 120.49 fs. After stretching by the glass rod, the pulse width broadened to 7.48 ps, consistent with the dispersive properties and length of the rod.

Since the stretched pulse width significantly exceeded the temporal intervals between modulated sub-pulses, autocorrelator measurements would cause overlapping signals from adjacent sub-pulses, rendering them indistinguishable. Therefore, we first modulated the unstretched pulse using the LC-SLM and characterized its autocorrelation signal to demonstrate the LC-SLM's pulse manipulation capability.

For the first modulation scenario, the initial pulse was split into a double-pulse sequence with a 1 ps interval by dividing the LC-SLM into two regions: the first region loaded with zero phase modulation and the second with phase modulation corresponding to a 1 ps delay, where Figure 3(c) displays the modulated autocorrelation signal showing a measured interval of 0.939 ps; in the second scenario, the initial pulse was split into a triple-pulse sequence with 1 ps intervals between consecutive pulses by partitioning the LC-SLM into three regions—applying zero phase modulation to the first region, 1 ps delay modulation to the second, and 2 ps delay modulation to the third—with Figure 3(d) showing the modulated autocorrelation signal revealing measured intervals of 0.978 and 1.059 ps. In both cases, the achieved pulse intervals deviated from the target 1 ps value by $\leqslant 6.1\%$, demonstrating the spatial light modulator's flexibility and precision in temporal pulse interval control.

Spatial resolution test of TT-STAMP

To further quantitatively evaluate the spatial resolution of the system, the USAF1951 resolution target was employed to test the lateral and longitudinal spatial resolution. Figure 3(e) shows ten frames of the third and fourth elements in Group 5 of the USAF1951 resolution target captured by the CCD, indicating that the lateral and longitudinal resolutions of the imaging results are essentially consistent. Figure 3(f) displays resolution curves in different directions, further quantitatively demonstrating the consistency between lateral and longitudinal resolutions. Although for a single image, the lateral and longitudinal resolutions are nearly identical, the highest resolution varies across images at different time points. As shown in Figure 3(g), due to the larger spot size after dispersion, images at the edges experience significant aberrations after passing through the lens periphery, resulting in better spatial resolution for the middle frames compared to the end

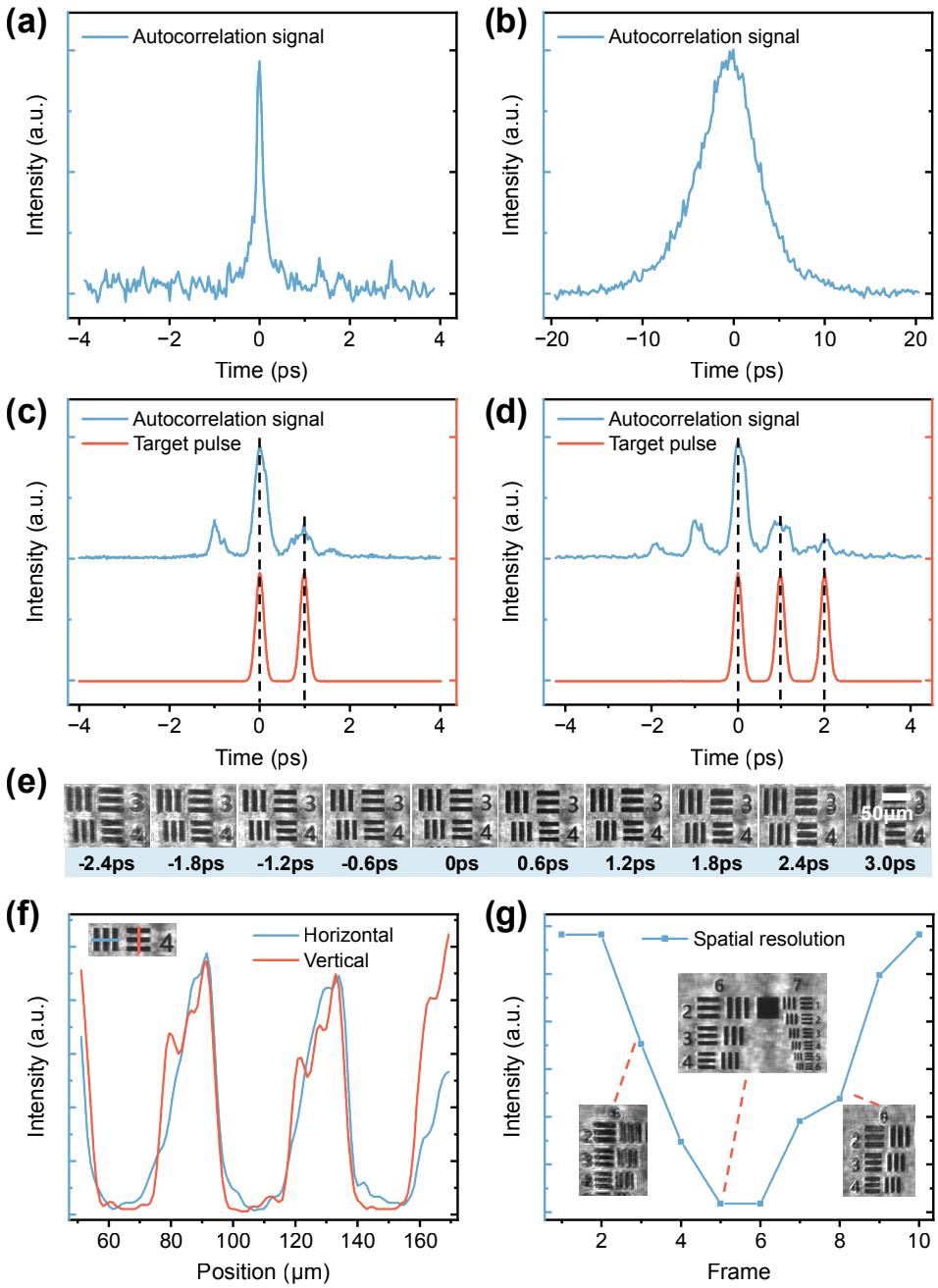

Figure 3 Testing and analysis of temporal and spatial resolution. (a) Pulse width measurement of the output light source using an autocorrelator. (b) Pulse width after stretching by the glass rod. (c) Double pulses with a 1 ps time interval. (d) Triple pulses with a 1 ps time interval. (e) Imaging performance tested using a resolution target (USAF 1951, Group 5). (f) Horizontal and vertical resolution test of the imaging system, showing consistent resolution in both dimensions. (g) Spatial resolution of each frame in a 10-frame sequence.

frames. Compared to the case without phase modulation, the minimum spatial resolution shows no significant change. Considering this phenomenon, it is advisable to use the middle frames for capturing more critical information during actual imaging.

Reconstructing dynamics of femtosecond laser-air interaction using TT-STAMP

To further demonstrate the flexible control capability of our proposed single-shot ultrafast imaging method with tunable time intervals over the sub-pulses, we reconstructed the dynamics of femtosecond laser-air interaction [22]. Taking the common phenomenon of femtosecond laser focusing-induced air filamentation as an example, a 200 μJ pulse was focused into a filament using a lens with a focal length of 50 mm. Different phase modulations were applied to the probe photon pulses, and the corresponding image information of each sub-pulse was captured. By comparing the filamentation variations between different frames, the control effect on the sub-pulses was reflected. In the experiment, the base time interval was 0.67 ps, and the number of captured frames was 10. To cover the entire ultrafast phenomenon, the fifth frame was set as the zero point, meaning that the sub-pulse corresponding to the fifth frame was synchronized with the pump pulse focusing to generate the plasma filament.

Figure 4 shows the overall control effect of the sub-pulses. Figure 4(a) presents the ultrafast images corresponding to the original unmodulated pulse sequence, where the air plasma filamentation phenomenon occurs in the 6th frame and concludes its growth process by the 9th frame, remaining stable thereafter. Based on the growth length of the plasma filament between frames and the corresponding inter-frame time intervals, the growth speed of the plasma was calculated to be approximately 1.82×10^8 m/s (as indicated by the slope of the dashed line in Figure 4(a)), close to two-thirds of the speed of light. This unmodulated phenomenon serves as the baseline for comparison and explanation of the observations under modulation. Additionally, for ease of analysis, a theoretical growth curve of the filamentation phenomenon after the corresponding modulation time is depicted with white dashed lines in each set of experimental images.

In Figure 4(b) and (c), the probe pulse was divided into two equal parts, with the first half left unmodulated while the second half was subjected to phase modulation. In Figure 4(b), a 0.5 ps delay modulation was applied to the second half of the pulse, whereas in Figure 4(c), a 1 ps delay modulation was introduced. This resulted in time intervals of 1.17 ps (0.5 ps + 0.67 ps) and 1.67 ps (1 ps + 0.67 ps) between the 5th and 6th frames, respectively, while the intervals between other frames remained at 0.67 ps. Compared to Figure 4(a), the entire growth-to-stabilization process of the plasma shifted forward, reducing from the original 4 frames to 3 and 2 frames, respectively. The observed phenomena closely matched the theoretical predictions.

In Figure 5(a), the probe pulse was segmented into three parts: the first part was unmodulated, while the latter two were independently modulated. Here, a 1 ps delay modulation was applied to the second segment and a 2 ps delay to the third segment. This created time intervals of 1.67 ps (1 ps + 0.67 ps) between the 3rd and 4th frames and another 1.67 ps (2 ps − 1 ps + 0.67 ps) between the 6th and 7th frames, with other intervals fixed at 0.67 ps. Relative to Figure 4(a), the overall plasma growth shifted forward, and the growth slope between the 4th and 6th frames aligned well with the calculated value of 1.82×10^8 m/s from Figure 4 (a). Between the 6th and 7th frames, the interval was 1.67 ps, yet filament stabilization was nearly achieved by 2.4 ps, yielding a growth speed of approximately 2.34×10^8 m/s. Again, experimental observations agreed with theoretical expectations.

In Figure 5(b), the probe pulse was similarly divided into three parts, but only the second segment was modulated with a 1.5 ps delay, leaving the first and third segments unaltered. This produced a 2.17 ps interval (1.5 ps + 0.67 ps) between the 3rd and 4th frames and a −0.83 ps interval (−1.5 ps + 0.67 ps) between the 6th and 7th frames, while other intervals remained at 0.67 ps. Notably, filament growth advanced to occur

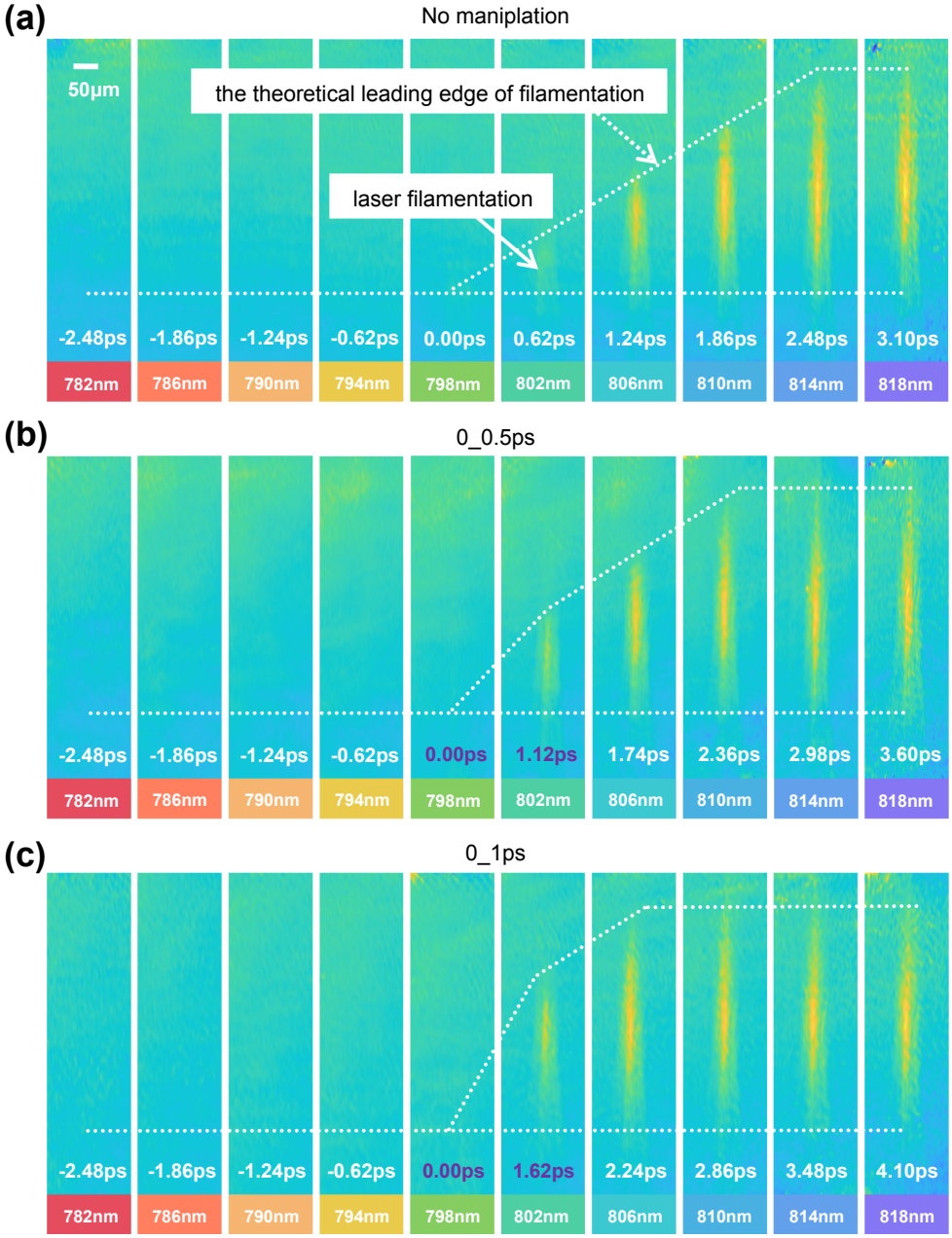

Figure 4 Air filamentation images with global time shifting using LC-SLM. The theoretical leading edge of filamentation is indicated by dashed lines. Each frame is labeled with time at the bottom, and the colored blocks at the bottom represent spectral distributions. (a) Unmodulated phenomenon. (b) With 0_0.5ps modulation: an additional 0.5 ps time interval is added between the 5th and 6th frames. (c) With 0_1ps modulation: an additional 1 ps time interval is added between the 5th and 6th frames.

between the 4th and 6th frames, whereas phenomena in the 1st–3rd and 7th–10th frames matched those in the corresponding frames of Figure 4(a), consistent with the theoretical outcome of selectively modulating the second segment. For clearer analysis, Figure 5(c) reordered the frames chronologically and plotted the filament growth curve against the adjusted time intervals, demonstrating close agreement between observations and theory.

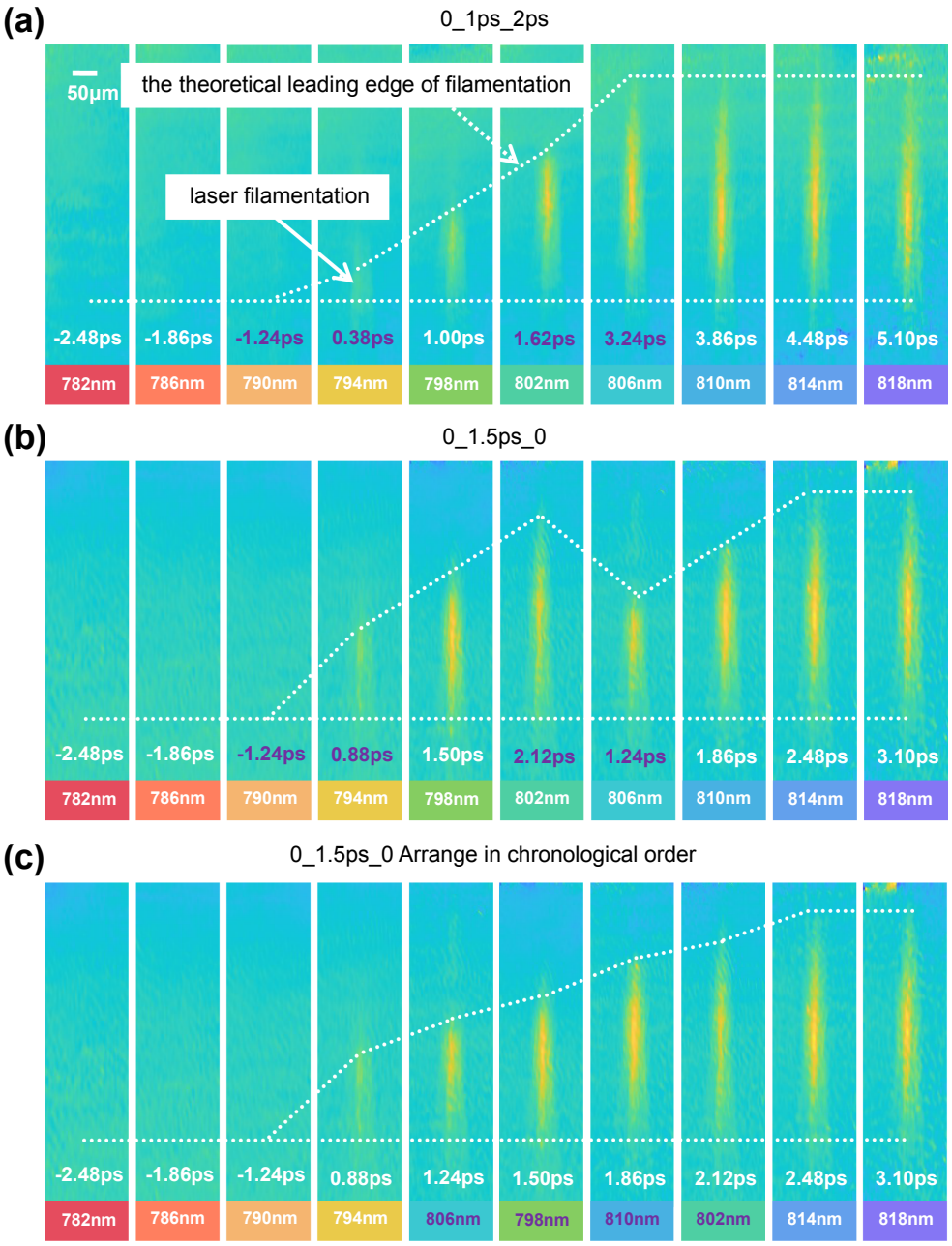

Figure 5 (a) With 0_1ps_2ps modulation: an additional 1 ps time interval is added between the 3rd and 4th frames, and another 1 ps time interval is added between the 6th and 7th frames. (b) With 0_1.5ps_0 modulation: an additional 1.5 ps time interval is added between the 3rd and 4th frames, while the originally added 1.5ps time interval is removed between the 6th and 7th frames. (c) The phenomenon in (b) rearranged according to chronological order.

DISCUSSION

The control capability of the LC-SLM over frames is a critical factor determining the temporal resolution of TT-STAMP. First, based on Yang et al.'s [21] analysis of ultrashort pulse temporal manipulation methods, the

temporal resolution of ultrashort pulse sequence shaping is limited by the resolution of LC-SLM and the spectral width of the probe pulse. Specifically, when introducing longer delays to sub-pulses within the TT-STAMP probe pulse sequence, extra-pulses emerge adjacent to the modulated sub-pulses. As the delay increases, the signal-to-noise ratio (SNR) of the probe pulse sequence deteriorates. Although employing higher-resolution LC-SLMs and broader-spectrum probe pulses can improve the temporal resolution of TT-STAMP, it cannot entirely eliminate the impact of these extra-pulses and noise.

Furthermore, two additional factors must be considered: (1) the temporal broadening caused by the reduced spectral width after dividing the probe pulse into multiple sub-pulses, and (2) the temporal stretching of sub-pulses due to the glass rod dispersive element. These effects may lead to overlapping between adjacent probe sub-pulses. While increasing the delay size could mitigate overlap, this approach is constrained by the system-dependent upper limit of achievable delays (as noted earlier). Thus, trade-offs are necessary when designing the number of spectral regions for LC-SLM subdivision, delay magnitude, and the dispersive element's properties, depending on the specific scientific objectives. Nevertheless, optimizing parameters such as LC-SLM resolution and probe pulse spectral width can significantly enhance the temporal resolution of the TT-STAMP system.

Data availability

The original data are available from corresponding authors upon reasonable request.

Funding

This work was supported by the National Key R&D Program of China (2023YFF0723300), the National Natural Science Foundation of China (62475198), the Fund of National Key Laboratory of Plasma Physics (6142A04230201), and the Shenzhen Science and Technology Program (JCYJ20230807090207014 and JCYJ20250604122706009).

Author contributions

Q.Y., K.Y., and C.L. proposed the idea; Q.Y. and K.Y. conducted the experiments; Z.Y., X.M., Q.Z., M.Y., and W.Y. provided assistance with the experiments; Q.Y. wrote the original draft; H.C., D.W., and C.L. supervised the project; all authors contributed to the review of the manuscript.

Conflict of interest

The authors declare that they have no conflict of interest.

References

1 Liang J, Wang LV. Single-shot ultrafast optical imaging. *Optica* 2018; **5**: 1113.

2 Wang P, Wang LV. Single-shot reconfigurable femtosecond imaging of ultrafast optical dynamics. *Adv Sci* 2023; **10**: 2207222.

3 Wang X, Yan L, Si J, *et al.* High-frame-rate observation of single femtosecond laser pulse propagation in fused silica using an echelon and optical polarigraphy technique. *Appl Opt* 2014; **53**: 8395.

4 Yuan X, Li Z, Zhou J, *et al.* Hybrid-plane spectrum slicing for sequentially timed all-optical mapping photography. *Opt Lett* 2022; **47**: 4822.

5 Chang C, Kuramochi H, Singh M, *et al.* A unified view on varied ultrafast dynamics of the primary process in microbial rhodopsins. *Angew Chem* 2022; **134**: e202111930.

6 Wu YL, Yu XH, Hasaien JZL, *et al.* Ultrafast dynamics evidence of strong coupling superconductivity in $LaH_{10\pm\delta}$. *Nat Commun* 2024; **15**: 9683.

7 Li Z, Lin J, Wang C, *et al.* Damage performance of alumina ceramic by femtosecond laser induced air filamentation. *Optics Laser Tech* 2025; **181**: 111781.

8 Sinha SK, Khammari A, Picher M, *et al.* Nanosecond electron pulses in the analytical electron microscopy of a fast irreversible chemical reaction. *Nat Commun* 2019; **10**: 3648.

9 Zhang Z, Qiu W, Zhang G, *et al.* Progress in applications of shockwave induced by short pulsed laser on surface processing. *Optics Laser Tech* 2023; **157**: 108760.

10 Betti R, Hurricane OA. Inertial-confinement fusion with lasers. *Nat Phys* 2016; **12**: 435–448.

11 Zylstra AB, Hurricane OA, Callahan DA, *et al.* Burning plasma achieved in inertial fusion. *Nature* 2022; **601**: 542–548.

12 Qi D, Zhang S, Yang C, *et al.* Single-shot compressed ultrafast photography: A review. *Adv Photon* 2020; **2**: 1.

13 Gao L, Liang J, Li C, *et al.* Single-shot compressed ultrafast photography at one hundred billion frames per second. *Nature* 2014; **516**: 74–77.

14 Cheng L, Qi D, Yao J, *et al.* All-optical discrete illumination-based compressed ultrafast photography. *ACS Photon* 2025; **12**: 5155–5164.

15 Dorozynska K, Kornienko V, Aldén M, *et al.* A versatile, low-cost, snapshot multidimensional imaging approach based on structured light. *Opt Express* 2020; **28**: 9572.

16 Ehn A, Bood J, Li Z, *et al.* FRAME: Femtosecond videography for atomic and molecular dynamics. *Light Sci Appl* 2017; **6**: e17045.

17 Saiki T, Hosobata T, Kono Y, *et al.* Sequentially timed all-optical mapping photography boosted by a branched 4f system with a slicing mirror. *Opt Express* 2020; **28**: 31914.

18 Nakagawa K, Iwasaki A, Oishi Y, *et al.* Sequentially timed all-optical mapping photography (STAMP). *Nat Photon* 2014; **8**: 695–700.

19 Li Z, Xiao L, Feng Z, *et al.* Sequentially timed all-optical mapping photography with quantitative phase imaging capability. *Opt Lett* 2024; **49**: 5059.

20 Li Z, Yuan X, Weng Y, *et al.* 2D spectrum slicing for sequentially timed all-optical mapping photography with 25 frames. *Appl Phys Lett* 2023; **123**: 141103.

21 Yang K, Xiao R, Zhou J, *et al.* Multidimensional ultrashort optical pulse manipulation using spatial light modulation. *Opt Lett* 2024; **49**: 4246.

22 Li YT, Xi TT, Hao ZQ, *et al.* Oval-like hollow intensity distribution of tightly focused femtosecond laser pulses in air. *Opt Express* 2007; **15**: 17973.